DOI : https://doi.org/10.56452/112

ISSN: 0974-5823 Vol. 7 (Special Issue 5, December 2022)

International Journal of Mechanical Engineering

Vibration Analysis for Damage Detection in Composite Plate by using Piezoelectric Sensors

Dr. Sarika Patil[1], Dr. Kishor. B. Waghulde[2], Dr. Vijaykumar Javanjal[3] Dr. Atul Patil[4] Dr.Vijay Baburao Roundal[5], Dr. Prathamesh Sudhakar Gorane[6]

[1]Associate. Professor, Department of Electronics and Telecommunication Engineering, DYPCOE, Akurdi, Pune, India

[2]Professor, Department of Mechanical Engineering, DIT, Pimpri, Pune, India

[3]Associate. Professor, Department of Mechanical Engineering, DIT, Pimpri, Pune, India

[4]Associate. Professor, Department of Mechanical Engineering, DIT, Pimpri, Pune, India

[5]Assistant Department of Mechanical Engineering, GSMCOE, Pune, India

[6]Assistant Professor, Department of Mechanical Engineering, GSMCOE, Pune, India

Abstract:

This study focuses on an active monitoring method for damage detection applied to composite structures. Different specimens made up of fiber epoxy resin in the form of composite structures arestudied. Wavelet analysis methods are adopted to post process the raw monitored signal. A new damage signature is introduced to determine the presence and extent of damage in composites, while eliminating the influence of different distances between the active actuator and active monitoring elements. The proposed method is shown to be effective, reliable, and straightforward for the specimens considered in the present study, which are composed of different materials and suffer various levels of damage. An online real-time active monitoringsystem for damage detection is described that is based on this research.

1. Introduction

On a macroscopic scale, composites have been around for centuries, whether in the form of straw-clay bricks or a concrete-aggregate roadway. In mechanical design applications, composites are engineered materials comprising reinforcement fibers, particles, flakes, and the like embedded in a supporting matrix of polymers, metals or ceramics. The matrix is the bonding element that can be shaped, while the reinforcement enhances the material properties of the matrix. Properly designed, the new material has properties superior to those of either original material alone, such as higher stiffness or better strength-to-weight ratios. The matrix component is usually an epoxy or polymide-resin that transfers the load between broken fibers and unbroken ones, and between fibers not oriented along the lines of tension. Fibers serve to resist tension, the matrix resists shear, and in combination, the new material resists compression. Such aerospace-grade materials are formed to the end-shape, and generally require heat and pressure for manufacturing. Molding and casting are two common processes, and the end product (individual layers or plies) can be further Lay up (laminated) to achieve final performance specifications. Each ply has its own material properties, fiber orientation, and thickness. Possible advantages of using composites as compared to traditional metals and alloys include reduced costs due to lower production costs, long-term durability and reduced maintenance requirements; lighter weight or the possibility to readily create non-uniform weight distributions; higher strength-to-weight ratios and directional strength or stiffness; the opportunity to design larger, single-piece parts with unusual geometries; corrosion or weather resistance; low thermal conductivity and coefficient of expansion; and non-magnetic, high-dielectric strength.

Structural health monitoring and damage detection [3] has been an important concern in the design, operation, maintenance, and repair of many military and civil structures and machinery equipment. Under scheduled maintenance conditions, damage detection has been accomplished with nondestructive inspection and evaluation techniques. Examples of these techniques include magnaflux, radiography, thermal imaging, acoustic microscopy, and various eddy current and ultrasonic methods. Damage detection techniques have also been developed for in-situ and in-service structural health monitoring. In principle, these techniques allow the detection of incipient damage in service environments by monitoring vibration characteristics, strain variations, acoustic emission, dielectric response, or electromechanical impedance of the host structure. The development of successful in-situ and in-service monitoring methods depends on two key factors: sensing technology and the associated signal analysis and interpretation algorithm. In the area of sensors, piezoelectric transducers have many advantages. They are active sensors in the sense that they can be used both to receive and generate signals, and their signals usually do not require conditioning treatment. In principle, these active sensors can perform two functions. In the passive mode, they can monitor dynamic events (e.g. foreign-object impact and damage-induced acoustic emission) by sensing the response of the structure. In the active mode, they can evaluate real-time structural properties and identify existing damage by sending and receiving programmed diagnostic signals [5].

2. Constitutive Equations of PZT Material

At low drive levels, piezoceramic materials exhibit nearly linear properties. A linear model is sufficient to characterize the dynamic behavior in these operating regimes. However, at moderate to high drive levels, the piezoceramic materials show nonlinearities and hysteresis. Applications at these drive levels need to consider the nonlinearities and hysteresis. Without considering structural damping and any constitutive nonlinearity, thermodynamic arguments based on Gibbs free energy and Maxwell's equation of electromagnetism yield the following constitutive equation for PZT

$$\sigma = c^P \varepsilon - \; c^P \beta P$$

$$P = x \in_0 \varepsilon + \gamma\sigma \qquad \text{…..2.1}$$

In this equation, σ, ε, E and P denote the stress, strain, electrical field and polarization in the PZT actuator, respectively. Symbols and descriptions of the coefficients are listed in Table 1. We can see that the relationship between P, σ, ε and E is linear. Also, we have the linear relation Q = Eh, where h is the thickness of the PZT across which the input voltage Q is applied. This equation applies at low input voltages, when hysteresis and nonlinearities are negligible.

SYMBOLS	DESCRIPTION
c^P	Young's modulus at constant polarization
β	Dielectric nonpermittivities under constant strain
x	Electric susceptibility
$\in_0$	Permittivity of free space
γ	Piezoelectric and electric coupling coefficient

Table 1: Symbols and descriptions of the coefficients

2.1. Nonlinear Presentation of Constitutive Equations

At moderate and high voltages, hysteresis is not negligible. To establish the nonlinear constitutive equation, it is assumed that the stress-strain relation is linear in the presence of the electrical field. However, the input voltage Q(t), the resulting strain ε and polarization P are assumed to exhibit hysteretic behavior. Thus we can write the polarization as a nonlinear function of the input electrical field and the generated stress, P = $\mathcal{F}$(E, ε), where, $\mathcal{F}$ quantifies the nonlinearity and hysteresis inherent to the materials. Further experiments show that

the relationship between the polarizations P and the generated strain or stress is linear, so the nonlinearity lies only in the relationship between the resulting polarization P and the input electrical field E. Including a structural damping term; we generalize Equation 2.1 as

$\sigma = c^P \varepsilon + C_D \dot{\varepsilon} - \ c^P \beta P$

$P = \ \mathcal{F}(E)$ **…..2.2**

In this equation, $C_D$is the Kelven-Voigt damping factor. The history dependent functional $\mathcal{F}$ (·) quantifies the intrinsic nonlinearity of the materials. There are numerous choices for the hysteresis functional$\mathcal{F}$. Two common choices include the Domain Wall Method and the Preisach method. In this dissertation, we are interested in developing a frequency-dependent hysteresis model based on the Preisach model. In next section, the Preisach method is reviewed.

2.2.Preisach Model

2.2.1 Fundamentals of the Preisach Model

The Preisach model, by its nature, is a superposition of simple nonlinear functional. Just as a periodic signal can be expressed as the sum of weighted basis functions, for example express a signal as a Fourier series. This method expresses hysteretic behavior as the superposition of basis functional. Because the response of the stack to an input voltage is a multi-valued mapping problem, we need to define a special basis. This basis, also termed as a kernel in the Preisach model, shows hysteretic behavior. Let C [0, T] denotes the space of continuous functions on [0, T]. For an input signal u ϵC [0, T] and an initial configuration ξ 2 {−1, + 1}, the kernel, denoted as 'k', is a mapping from C [0, T] to {−1, + 1}. For a pair of threshold (β, α), with β ≤α, where α and β are all ϵ C [0, T]. The hysteresis is expressed as $[h(\mathcal{U}, \xi)](t) = \int_{\bar{P}} [\kappa_{\beta,\alpha}(\mathcal{U}, \xi)(t)\, d\mu$ **….2.3**

Where, μ(β, α) is a weight function, also referred to as a density function, which depends on the physical properties of the material. The kernel $\kappa_{\beta,\alpha}$(u, ξ) is a relay operator, also called a Preisach operator. The Preisach plane, is defined as

$$\overline{P0} \triangleq \{(\beta, \alpha) \epsilon \mathbb{R}^2 : \beta \leq \alpha\}$$

Which is an unbounded half-plane contained in is a bounded, triangular region in$\mathbb{R}^2$.The density function μ(β, α) is usually assumed to have compact support. For some value β < β0 and α > α0, the contribution of μ is very small, so we let μ ≡ 0at those values. We therefore define a new Preisach plane is a bounded, triangular region in$\mathbb{R}^2$.

$$\overline{P0} \triangleq \{(\beta, \alpha) \epsilon \bar{P}0 | \beta \leq \alpha, \beta \geq \beta_0, \alpha \leq \ \alpha_0\}$$

2.2.2 Discretization of the Preisach Plane

For the purpose of simulation and identification, the Preisach plane often needs to be discrete. The Preisach model is approximated by an expression having the for

$[(h_m \mathcal{U}, \xi)](t) = \quad \sum_{i=1}^{m} [k_{ni}(\mathcal{U}, \xi_{ni})](t) \omega_{ni}$ **….2.4**

Where, nithis is a node in the finite Preisach plane. The termω_{ni} is a weight value, andis defined in the summation

$$\mu = \sum_{i=1}^{m} \omega_{ni} \delta_{ni}$$

Where,δ_{ni} is the Dirac delta concentrated at node ni. In computational studies, we use$\bar{S}$ instead of.$\bar{P}, \bar{S}$is defined as

$$\bar{S} \ \triangleq \{(s_1, s_2) \in \mathbb{R}^2 | s_1 = \ s_{min} + \ (j-1)\Delta_{s,\ s2} = \ s_{min} + \ (k-1)\Delta_s, j \leq k\}$$

Where, j and k are integers. $\Delta_s$is defined as Δ_s=(s_{max}−s_{min})/N. s_{max} , s_{min}) is quantized uniformly into N pieces. The two thresholds β and α are denoted as $s_1 and\ s_2$ respectively. The two limits β_0 and α_0 are denoted as s_{min} and s_{max} respectively.

$[u_{min}u_{max}]$ is a strict subset of $[s_{min}s_{max}]$, where $[u_{min}u_{max}]$ is the input range of the system.

The smaller the $\Delta_s$is, the better simulation result can be achieved due to the increased resolution. The trade off is that it significantly increases the computation time. This method of approximation has nice convergence properties under mild assumptions.

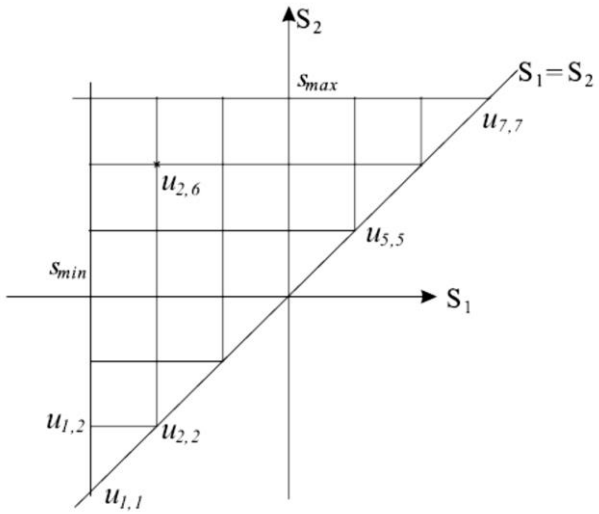

Figure 2.1: Discretization of the Preisach Plane

2.2.3. Recursive Definition of Hysteresis

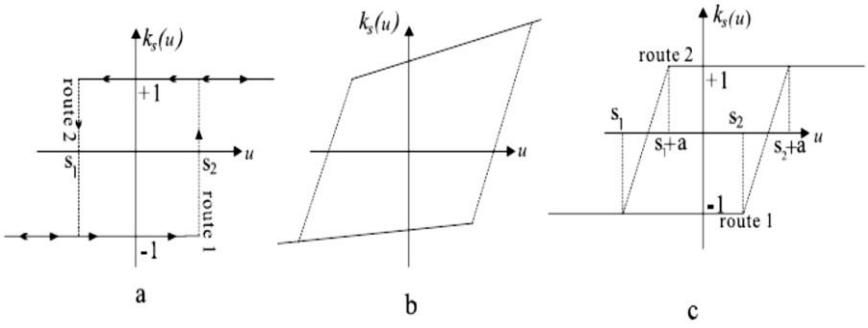

Figure 2.2: Preisach kernels

The original kernel employed in the Preisachmodel is as depicted in Figure 2.2 a, where s_1 and s_2 are the two thresholds of the relay operator, with $s_2 \geq s_1$. The symbol u(t) is the input of the system, and is continuous in time space.Assume at initial time t_0, the system input $u(0) \leq s_1$, the hysteresis kernel$k_s(u,t)$has value of -1. If the input u (t) monotonically increases, k_s remains at -1 until the input reachess_2, and then the response switches to +1. If the input starts from $u(0) \geq s_2$, and decreases monotonicallyk_s, remains at +1 until the input reachess_1, and then $k_s$switches to -1.

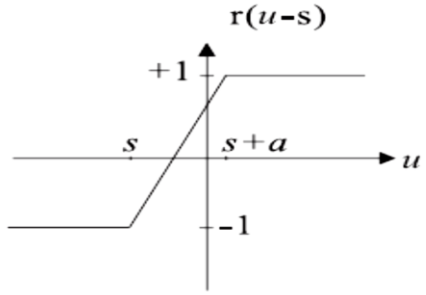

Figure 2.3: Ridge Function

$$k_s(u,t)=\begin{cases}-1 & u \le s \\ \frac{2}{a}(u-s)-1 & s \le u \le s+a \\ +1 & u \ge s+a\end{cases}$$

But as can be seen from the figure directly, this mapping from time to the value of the kernel is not continuous. This can be undesirable in practice. There are two other candidate kernels for Preisach model, which are shown in Figure 2.2 and 2.3. The kernel depicted in Figure 2.3 is the well-known Krasnolselskii–Pokrovskii operator, or KP kernel. KP kernel is widely used in mathematical models. To define the KP kernel, we first introduce a ridge function rs = r(u−s). The KP kernel is comprised of two ridge functions rs_1 = r(u − s_1) and rs_2 = r(u − s_2), with $s_2 \ge s_1$. Figure 2.3 depicts a plot of a single ridge function. The slope of the ridge function is determined by a. The input-output relationship associated with the KP kernel in Figure 2.3 is described as follows: when the input monotonically increases from u≤ s_1, the output follows path 1, when it decreases from u≥ (s_2 + a), the output follows path 2, for an input signal as in figure 2.4, if a monotonically increasing input decreases before it reaches s_2 + a, $k_s$takes the minimum of the current value and the upper envelope route.

The relation between the input and output is described as follows:

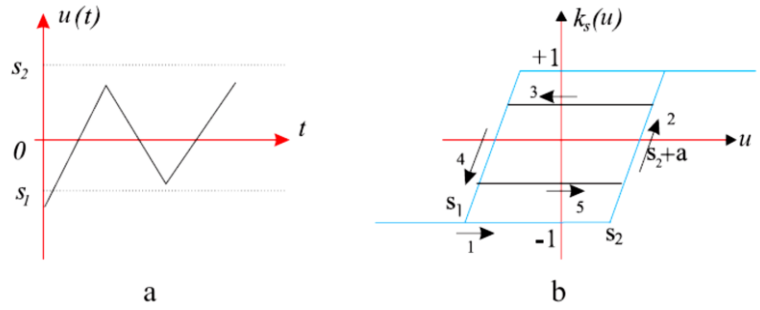

Figure 2.4: Major loop and minor loop

If a monotonically decreasing input increases before it reachess_1, $k_s$takes the maximum of the current value and the lower enveloped curve, as depicted in Figure 2.4. The upper and lower enveloped curves define the hysteresis major loop. The path consisting of (2), (3), (4) and (5) define a hysteresis minor loop. The mathematical expression for the hysteresis operator is given in Equation 2.5

$$[R(u,R_{k-1})](t)=\begin{cases}\{\max\{R_{k-1},r(u(t)-s_2)\}, if\ u\ is\ non-\ decreasing \\ \{\min\{R_{k-1},r(u(t)-s_1)\}, if\ u\ is\ non-\ increasing\end{cases} \quad 2.5$$

Where, R is defined by Equation 2.6.

$$[R_k](t)\begin{cases}R\{u,R_{k-1}(t_k)\}, k=2,3\ldots.j \\ R_0=\xi, k=1, \xi \in \{-1+1\}\end{cases} \textbf{.....2.6}$$

The initial condition is given by R0 = ξ. Definition 2.5 and 2.6 ensure that the minor loops rest inside the major loop.

2.3.Developing the Frequency Dependent Model

The research in this dissertation develops a frequency-dependent hysteresis model.

As noted in the domain wall model, with an input voltage Q(t), the generated electrical field is *E* (t) = Q(t)/d, where d is the thickness of the PZT. The electrical field E generates a polarization P = $\mathcal{F}$ (*E*). The polarization, conversely, generates an electrical field. The total electrical field, denoted as effective electrical fieldE_e is expressed as E_e = *E*+ αP and effective charge displacement is De = ε*E*+ P.

In these expressions, α is an inter-domain coupling factor and ϙ is the dielectricity of the material. So both E_e and D_e have hysteretic behavior. In Equation 2.2, the nonlinear constitutive equation can also be written as

$$\sigma = c^P\varepsilon + c_D\dot{\varepsilon} - c^P\beta D_e(E)$$

$$D_e = \mathcal{F}(E) \textbf{.....2.7}$$

$$\sigma = c^E\varepsilon + c_D\dot{\varepsilon} + E_e(D)$$

$$E_e = \mathcal{F}(D) \text{.....} \mathbf{2.8}$$

In equation 2.7 and 2.8, E_e and D_e denote the effective electrical field and effective charge displacement, respectively.

3. Review of Vibration and Waves Principles

The study of propagating waves has preoccupied many researchers. Early work was carried out by luminaries such as Lord Rayleigh and Lamb [2]. Because of the mathematical simplicity, the wave propagation in strings and rods was studied first and the equations of motion were developed. Later, the results were used for more complicated cases of waves propagating in infinite or semi-infinite media such as plates and membranes. In the last few decades, the guided wave propagation and the equations of motion was the focus of many researchers. The properties of guided waves have made them suitable to be used in the inspection techniques of metallic structures [1] and, in the last few years, they become predominant in the NDE and SHM applications.

3.1 Review of Wave Propagation Theory

Waves are disturbances that travel, or propagate, from one region of space to another. A classification of different types of waves propagating in elastic solids is presented below.

3.1.1 Pressure Waves

Pressure waves are also called compressional, axial, dilatational, longitudinal or P waves. For this type of wave motion, the particle displacement is parallel to the direction of propagation. The particle displacement in a pressure wave can be written as:

$$u_x(x,t) = u_0.\, e^{i(kx-wt)}$$

Where, *k* is the wave number, and ω is the angular frequency. The wave number can be written in terms of the wave speed (*c*) and the angular frequency (ω) as:

$$k = \frac{w}{c} = \frac{2\pi}{\lambda}$$

The particle displacement can be also written in terms of the wavelength γ.

$$u_x(x,t) = u_0.\, e^{iw\left(\frac{x}{c}-t\right)} = u_0.\, e^{i2\pi\left(\frac{x}{\lambda}-\frac{t}{T}\right)}$$

Where, $\gamma = cT$, $T=1/f = 2\pi/\omega$ is the period of oscillation. The wave speed (*c*) is calculated using various formulas, depending on the specific assumptions and the boundary conditions. For a three-dimensional free solid, the wave speed for a pressure wave is:

$$C_p = \sqrt{\frac{\lambda + 2\mu}{\rho}}$$

3.1.2 Shear Waves

Shear waves are also called transverse waves, distortional waves, or S-waves. For this type of wave motion, the particle displacement is perpendicular to the direction of wave propagation. The particle displacement can be written as:

$$u_y(x,t) = u_0.\, e^{i(k_S x-wt)}$$

In terms of the Lamé constants the wave speed of the shear waves can be written as:

$$c_S = \sqrt{\frac{\mu}{\rho}}$$

3.1.3 Flexural Waves

Flexural waves appear due to bending action. The Bernoulli-Euler beam theory assumes that plane sections remain plane after deformation. The Kirchhoff plate theory assumes that straight normal planes to the mid-surface remain straight after deformation.

3.1.4 Rayleigh Waves

Rayleigh waves are also known as surface waves. They propagate close to the body surface, with the motion amplitude decreasing rapidly with depth. The polarization of the Rayleigh waves lies in a plane perpendicular to the surface. The effective depth of penetration is less than a wavelength. The two components of the Rayleigh wave *ux*and *uy*can be calculated using an approximated equation for the wave velocity:

$$C_R = C_S\left(\frac{0.87 + 1.12v}{1 + v}\right)$$

The Rayleigh wave number and the components *ux*and *uy*are:

$$u_x(x,y,t) = u_0 k_R(e^{-qy} - \frac{2qs}{k_R^2 + s^2}e^{-sy})e^{i(k_R x - wt)}$$

$$u_y(x,y,t) = iu_0 q(e^{-qy} - \frac{2k_R^2}{k_R^2 + s^2}e^{-sy})e^{i(k_R x - wt)}$$

Where $q = \sqrt{k_R^2 - k_P^2}$ and $s = \sqrt{k_R^2 - k_S^2}$

3.1.5 Lamb Waves

Lamb waves are guided waves between two parallel free surfaces, such as the upper and lower surfaces of a plate. The displacements *ux*and *uy*are calculated as:

$$u_x = i.\left[\xi\left(Asin\,\eta_p y + Bcos\,\eta_p y\right) + \eta_s(C\,cos\,\eta_s y - Dsin\,\eta_s y)\right].e^{i\psi}$$

$$u_y = \left[\eta_p\left(Acos\,\eta_p y + Bsin\,\eta_p y\right) + \xi(C\,sin\,\eta_s y - Dcos\,\eta_s y)\right].e^{i\psi}$$

Where, $\psi = \xi x - \omega t$. The two non-zero stresses are:

$$\sigma_{yy} = (\lambda + 2\mu).\left(\frac{\partial^2\phi}{\partial x^2} + \frac{\partial^2\phi}{\partial y^2}\right) - 2\mu\left(\frac{\partial^2\phi}{\partial x^2} + \frac{\partial^2 H_z}{\partial x \partial y}\right)$$

$$\sigma_{xy} = 2\mu.\left(\frac{\partial^2\phi}{\partial x \partial y} - \frac{\partial^2 H_z}{\partial x^2} + \frac{\partial^2 H_z}{\partial y^2}\right)$$

Lamb waves can exist in two basic types: symmetric and antisymmetric. For each propagation type, a number of modes exist, corresponding to the solutions of the Rayleigh-Lamb equation. The symmetric modes are designated S0, S1, ….., while the antisymmetric modes are designated A0, A1, …..The particle motion for the two cases, symmetric and antisymmetric is presented in

DOI : https://doi.org/10.56452/112

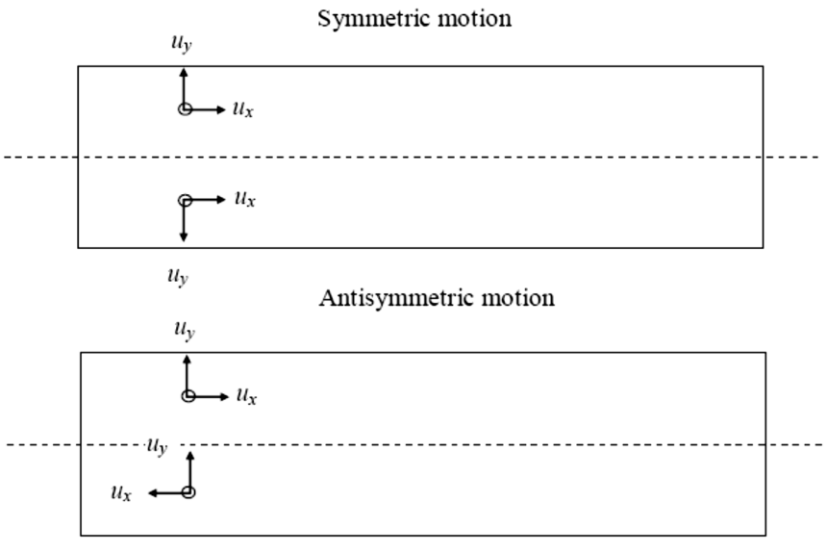

Figure 3.1: Symmetric and Antisymmetric Particle Motion across the Plate Thickness

4. Piezoelectric Wafer Active Sensors

Piezoelectric wafer active sensors (PWAS) are inexpensive permanently-attached small transducers (Figure 4.1) that operate on the piezoelectric principle [4]. The direct piezoelectric effect is manifested when the applied stress on the sensor is converted into electric charge. Conversely, the inverse effect will produce strain when a voltage is applied to the sensor. In this way the PWAS can be used as both transmitter and receiver of elastic waves [6].

The same sensors are used for both exciting (actuating) and reading (sensing) the received signals. Other advantages of using piezoelectric wafer active sensors for structural health monitoring are:

• PWAS are small, non-intrusive, and inexpensive intimately affixed to the structure and can actively interrogating the structure.

• PWAS are non-resonant devices with wide band capabilities. They can be wired into sensor arrays that are connected to data concentrators and wireless communicators.

• PWAS have captured the interest of academia and industry due to their low cost and non-intrusive nature.

4.1 Principle of Piezoelectric Wafer Active Sensors

Piezoelectric wafer active sensors (PWAS) operate on the piezoelectric effect: (a) direct effect – applying stress on the surface of a piezoelectric material will generate an electric field; (b) *indirect effect* – an electric field applied to a piezoelectric material will cause the material to contract. PWAS can be manufactured in thin layers of lead zicronatetitanate (PZT) material and can have various shapes (discs, rectangles, etc.) A piezoelectric wafer active sensor (PWAS) is permanently bonded on the surface of a structure through a layer of adhesive as shown in Figure 4.1 The PWAS interacts with the structure through the adhesive layer. The adhesive layer acts as a shear layer and is transmitting the mechanical effects from the PWAS to the structure and vice versa through shear effects.

DOI : https://doi.org/10.56452/112

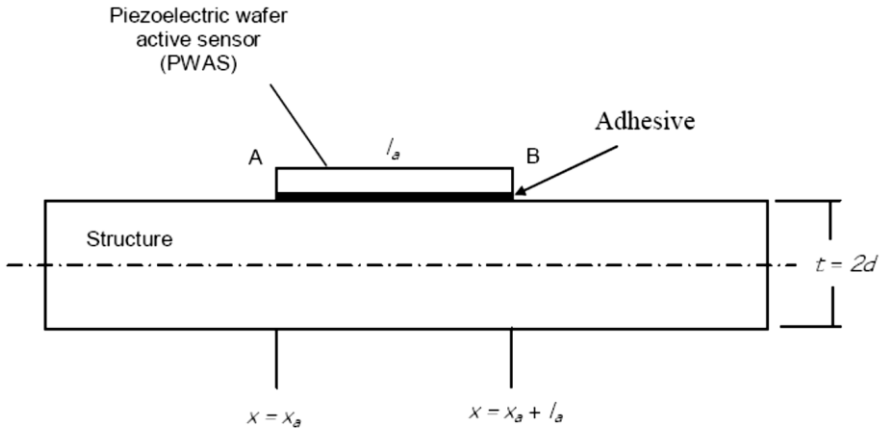

Figure 4.1: PWAS Attached to the Structure

The effect of such an interaction is the generation of elastic waves that travel through the structure to which the PWAS is affixed (Figure 4.2).

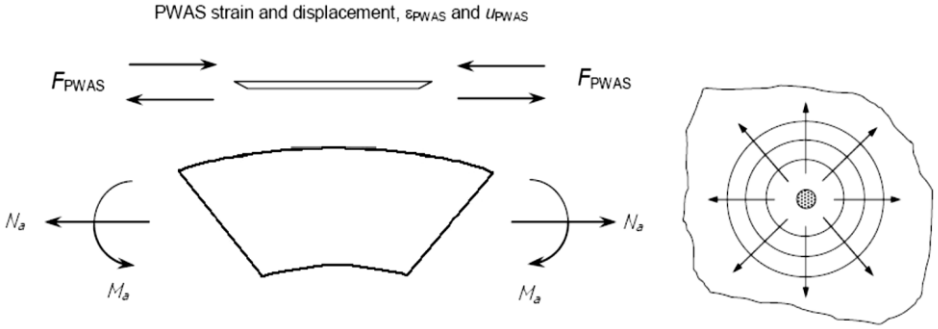

Figure 4.2: PWAS Interaction with Structure: Moments and Forces Circular Crested Lamb Waves Generated in a Two-Dimensional Structure

4.2 Attachment of Piezo Electric Element

Attaching a piezo element to the object is not to be performed with common soldering techniques. The soldering process must be done very carefully, not to cause any unwanted amplitude modulation (sidebands).

4.2.1 Soldering of the Cables

The piezo ceramic takes harm of high temperatures, so using a technique where the object to be soldered on is heated until the soldering tin melt with contact to the object, is not to prefer. Only a few seconds contact with the soldering pen is recommended. But the surfaces are prepared for such soldering and the soldering tin can almost be painted on with a thin layer. Try not to take too much soldering tin or to get porosities or flaws in the soldering.

4.2.2 Gluing of Piezo Elements

Gluing of piezo elements should not be performed as in ordinary modal analysis where a thin glue layer is preferred. The glue layer must be thick not to produce unwanted nonlinearity. The glue shall also rather be soft than hard, to get a smooth transfer of the signal without any produced non-linearity. Let the glue dry for a short while before using it so it does not float out when putting it on the test object. Further let it dry a while more on the test object so the piezo elements do not sink toward the test object and get in contact with it when attaching it.

DOI : https://doi.org/10.56452/112

4.2.3 Cables

Cables should be glued to the test object in a way that no tension in the cables occur making the amplitude of the piezo vary and produce sidebands. Further the cables shall be very thin not to affect the piezo element with its weight. A small drop of glue shall also be put on the solder of the cables on the upper side to fix it steady to the piezo.

4.2.4 Placement of Piezo Electric Elements

Placement of piezo elements is an important question. What can be said for sure is that same positions must be chosen for every test object if the amount of sidebands should be set in relation to the amplitudes in the low frequency components. The piezo element of course captures different amounts of different modes of vibration for different positions. The piezo elements still capture the low frequencies from the hammer hit very well.

Vibrations are also to some extent captured even in directions perpendicular to the polarisation of the piezo element. Instead the hammer hit often causes a problem with overloading of the scope. Of course a filter can be used to avoid this, but then measuring the hammer hit energy appropriately becomes a problem. Filter compensation is of course sometimes suitable.

The piezo element connected to the oscilloscope is best placed at a location where low amplitudes of vibrations are present. On rotor blades the root is a good place in order to not get too high amplitudes from the hammer hit see the other piezo element used for exciting the object with the ultrasound frequency should of course not be placed too close to the receiving piezo. If the piezo is very close, too much of the signal will go directly into the receiving piezo and the sideband frequencies will not appear as significant as the ordinary ultrasound signal if the material has high damping. This might disrupt the results if the sidebands are measured in proportion to the amplitude of the high frequency signal.

5. Experimental System Development

This section discusses the process of manufacturing the composites as well as the components of the experimental systems, the type of actuation signal employed, and post processing of the actively monitored signal, development of the new damage signature, and test results. A Teflon slice having dimensions (50x50) mm are embedded in composite plate at the time of manufacturing the specimens this embedded Teflon sheet considered as a type of delamination or damage in composite plate.

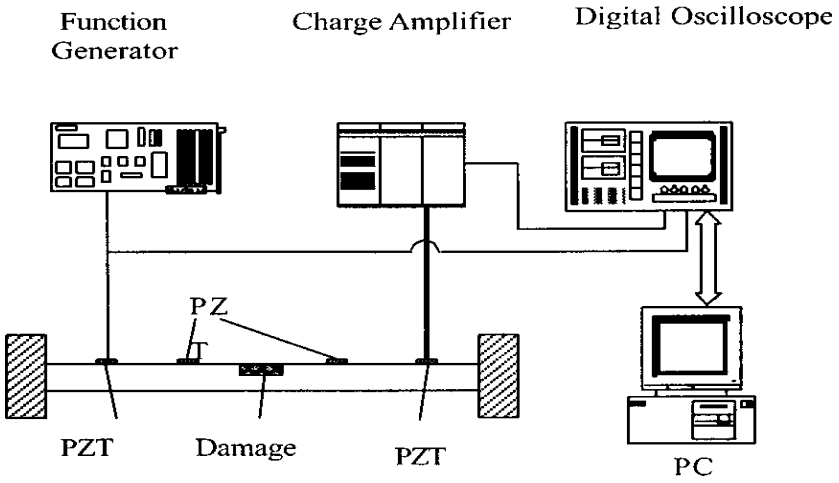

Figure.5.1: Experimental Setup

Experimental Setup Consists of:

1. Function Generator : ME 916 (6MHz)
2. Digital Storage Oscilloscope **: SCIEN**TECH 7100C (100MHz) Dual Trace
3. PZT Mounted Specimens : PZT Actuators And Sensors

Computer System : Core i3 2nd Generation Laptop**5.1 Development of Specimens**

DOI : https://doi.org/10.56452/112

Figure 5.2: Preparing the Mould for Specimens.

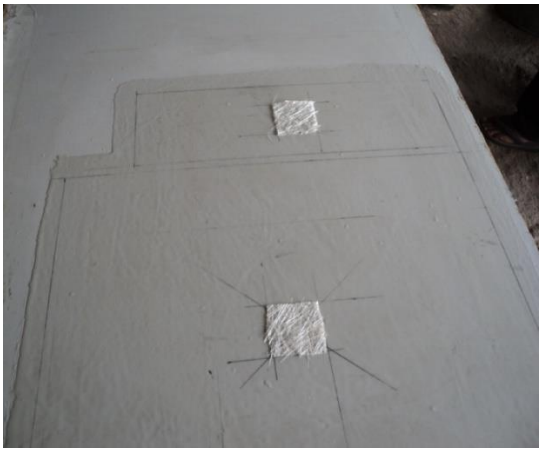

Figure 5.3: Applying the Hardener for Teflon Slice

Figure 5.4: Prepare the First Layer of Resin and Placing the Teflon Slice on It

DOI : https://doi.org/10.56452/112

Figure 5.5: Cutting the Glass Fiber Sheet as Per Requirement

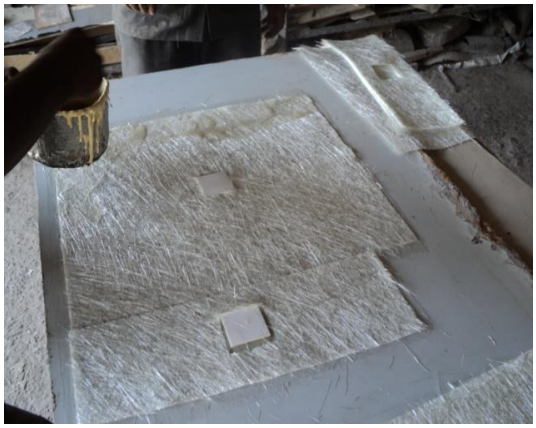

Figure 5.6: Applying the Alternate Layer of Resin and Glass Fiber Sheet.

Figure 5.7: Keep the Specimens for Curing and Cut Them as Per the Required Dimensions

DOI : https://doi.org/10.56452/112

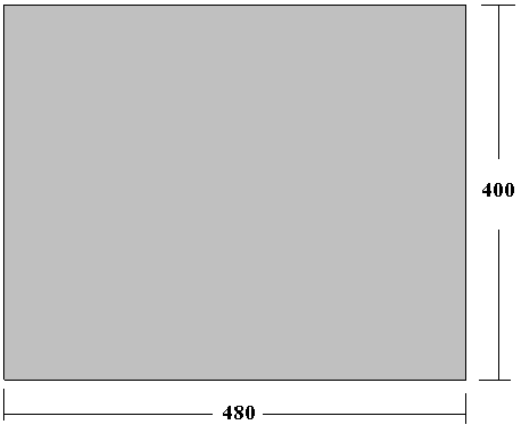

Figure 5.8: Specimen without Delamination

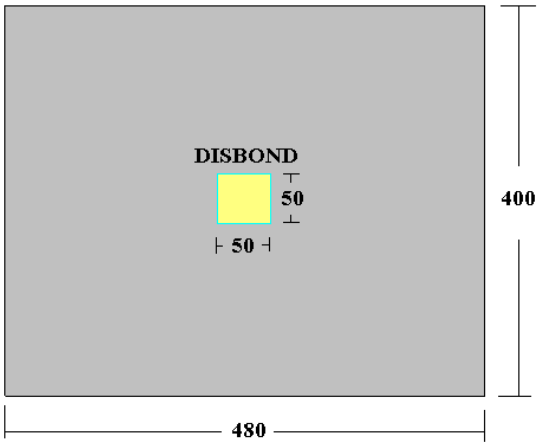

Figure 5.9: Specimen with Centered Square Delamination

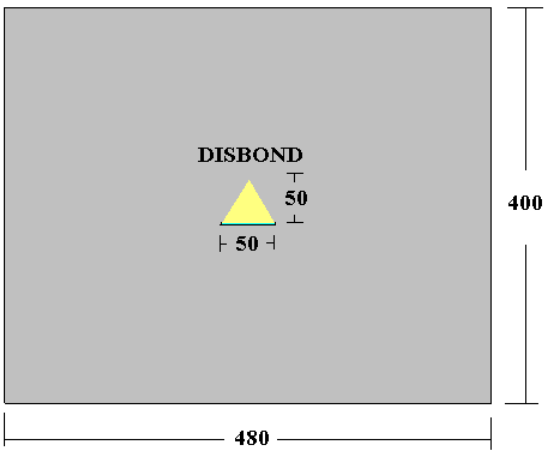

Figure 5.10: Specimen with Centered Triangular Delamination

DOI : https://doi.org/10.56452/112

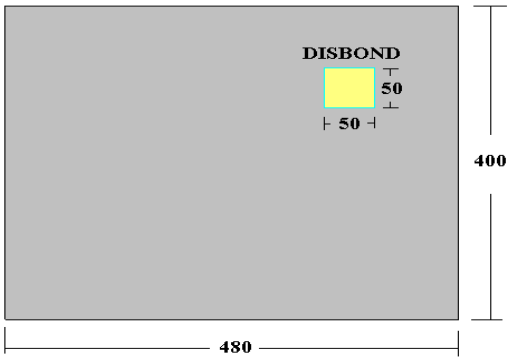

Figure 5.11: Specimen with Outline Square Delamination

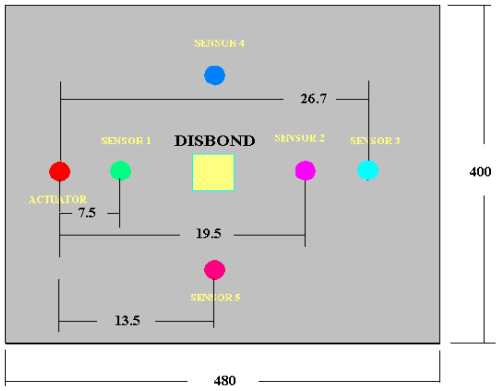

Figure 5.12: Position of Sensors on Plate

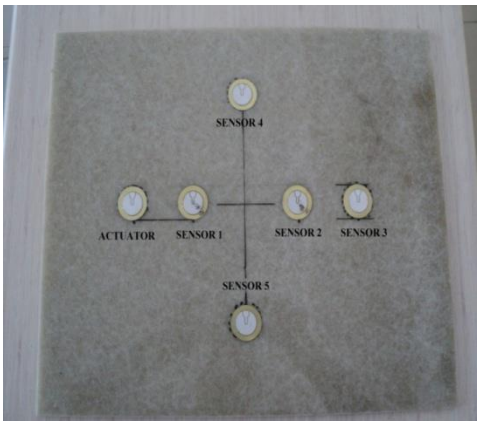

Figure 5.13: Actual Specimen without Delamination

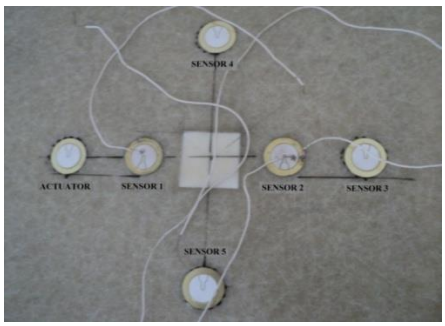

Figure 5.14: Actual Specimen with Centered Square Delamination

DOI : https://doi.org/10.56452/112

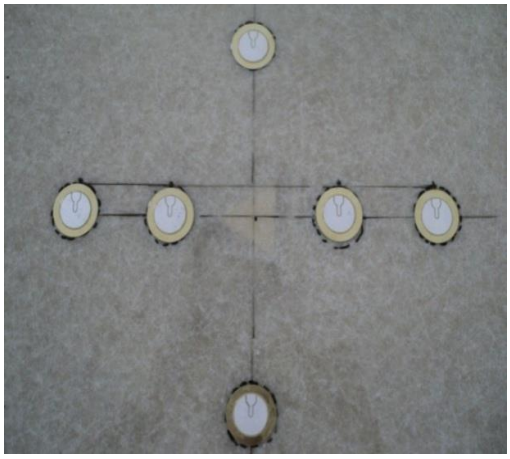

Figure 5.15: Actual Specimen with Triangular Delamination at Centre.

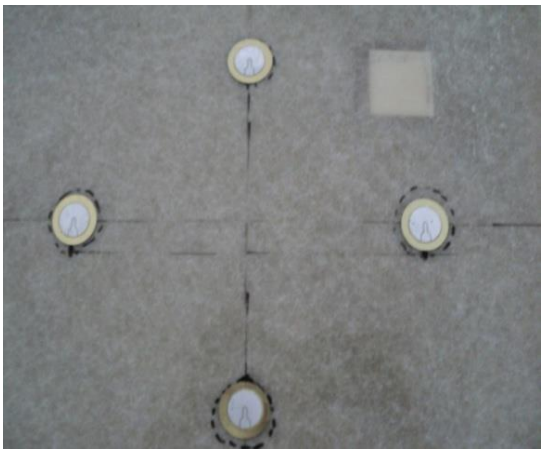

Figure 5.16: Actual Specimen with Outline Delamination.

5.1.1 Paths of Lamb Waves Propagation and Overall Part Coverage

In the experimental configurations Lamb wave propagation is used to perform instantaneous baseline structural health monitoring. Lamb waves are excited in a round robin fashion such that each PZT transducer acts as both a sensor and an actuator. For example, PZT 1 will act as an actuator and excite a Lamb wave in the plate while the surrounding transducers will act as

sensors, recording response data. PZT 2 will then act as an actuator and the surrounding transducers will act as sensors. This process is repeated until Lamb waves traveling along each path are recorded. Three different path lengths are used in the square configuration and six path lengths are used in the circular configuration. The individual path lengths as well as the total part coverage can be seen in Figure. 5.17 For the square pattern and in Figure. 5.18 For the circular pattern. For each PZT used as an actuator, not all of the remaining transducers are used to collect response data.

DOI : https://doi.org/10.56452/112

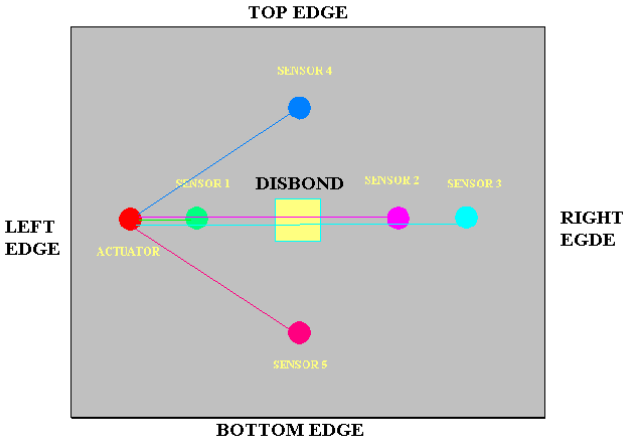

Figure 5.17: Paths of Lamb Waves

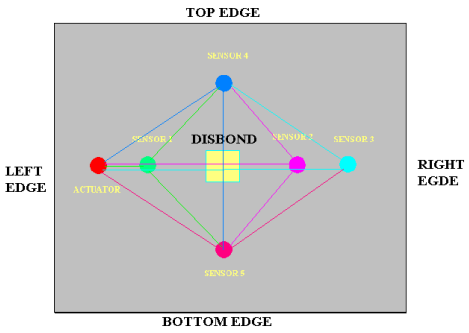

Figure 5.18: Overall Part Coverage

	TIME (MICRO SECONDS) for reflections from				
SENSOR NO.	LEFT EDGE	RIGHT EDGE	TOP EDGE	BOTTOM EDGE	DISBOND
SENSOR 1	100	362.5	175	202.5	107.5
SENSOR 2	172.5	292.5	175	202.5	37.5
SENSOR 3	292.5	172.5	175	202.5	37.5
SENSOR 4	362.5	100	175	202.5	107.5
SENSOR 5	162.5	162.5	62.5	310	90
SENSOR 6	162.5	162.5	281.5	68.5	90

Table 5: Time of Reflection from Plate Edges for Each Sensor.

DOI : https://doi.org/10.56452/112

5.1.2 Simulation of Reflections from Plate Edges

The energy of the signal traveling along the bond line is less than the energy of the signal traveling outside the bond line: the signal is weaker because the adhesive layer is absorbing part of the energy of the transmitted wave. For a better understanding of the complexity of wave propagation in the bonded structure and the multiple reflections that will arrive at the same time or very close to each other, a simulation of the reflections arriving at each sensor was done.

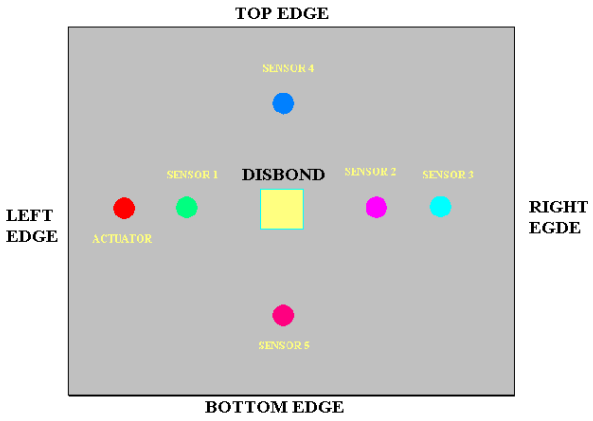

Figure 5.19: Simulation of Reflections from Edges

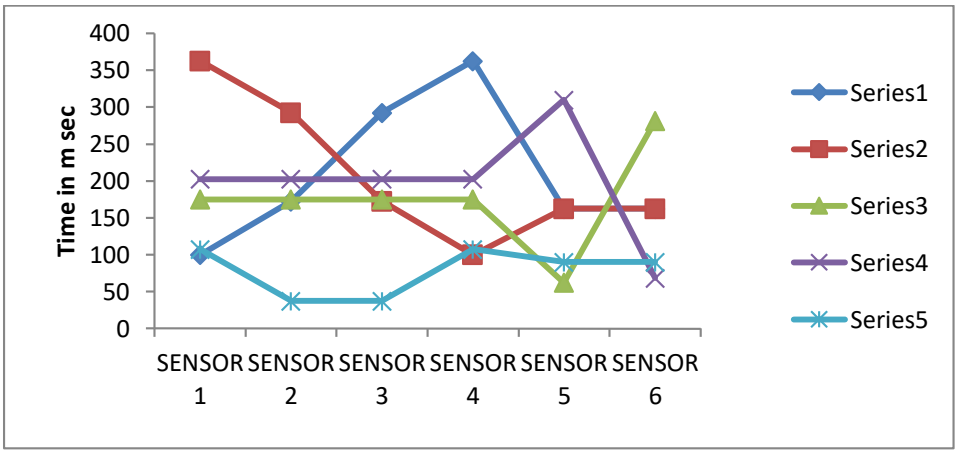

Figure 5.20: Reflections from Plate Edges for Each Sensor

From figure 5.20 it can be seen that multiple reflections will arrive at the same time and they will overlap making the identification process difficult. Sensor located to the right of the first disbond, we see between 100m sec and 150m sec that there are three reflections that will overlap: (i) reflection from the right edge of the specimen; (ii) reflection from the top edge of the specimen and; (iii) the reflection from the disbond. In order to eliminate some of the reflections from the edges of the specimen, non-drying modeling clay was used on the periphery of the specimen.

5.2 Selection of Active Actuation Signal

The type of active actuation signal used in the damage identification process is very important. The actuation signal can vary from conventional constant amplitude sinusoidal waves to bursts, sweeps, impulses, etc. In this research, the actuation signal should be broadband. Thus, an impulse signal is attractive. There are three aspects of such an impulsive signal that need to be determined: shape, width and amplitude. Because the

structure is linear and vibration amplitudes should be small, the amplitude of the impulse can be somewhat arbitrarily specified. In this study, impulses with a half-sine wave and a rectangular shape are tested on the specimens considered.

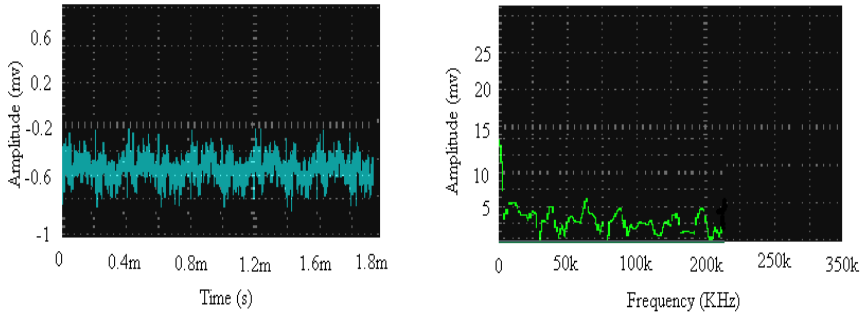

Figure 5.21: Active Monitoring Signal under Half-Sine Wave Actuation

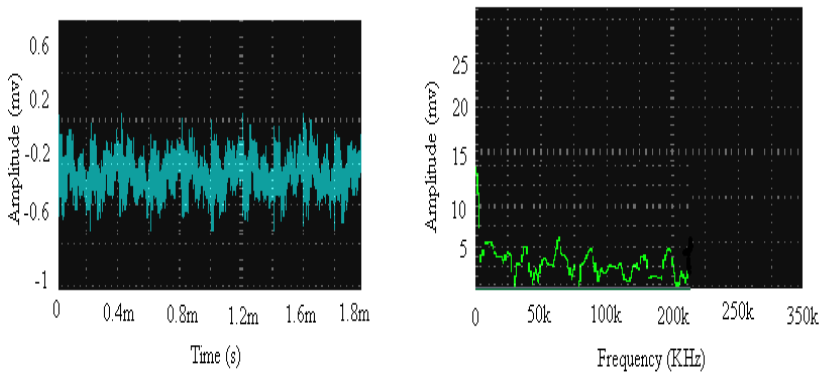

Figure 5.22: Actively Monitored Signals under Rectangular Impulse Actuation

Comparing these experimental results, conclusions can be drawn as follows. First, in the time domain, the peak value of the actively monitored signal for the half-sine impulse actuation is smaller approximately half of that of the rectangular impulse. Second, while the cut-off frequency for both of the actuation signals is about 50 kHz.

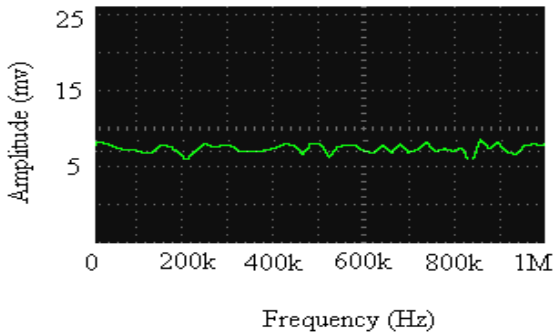

Figure 5.23: Frequency Analysis Results of Active Monitoring Signal under 500 ns-wide Impulses

DOI : https://doi.org/10.56452/112

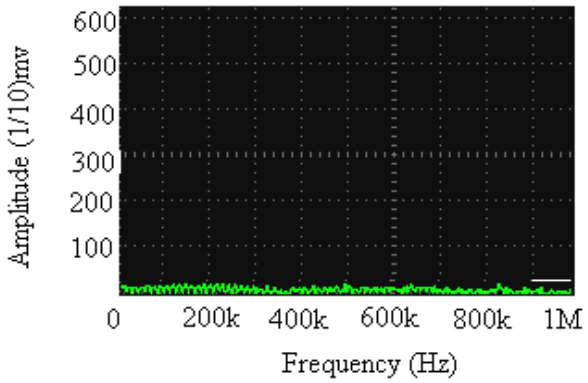

Figure 5.24: Frequency Analysis Results of Active Monitoring Signal under 10 μs -wide Impulse5.3 Post Processing of the Actively Monitored Signal

Experimental results show the actively monitored signal is very repeatable. However, even under laboratory conditions, noise is still present, including a 50 Hz electric line noise. The sensitivity of piezoelectric elements is very high. These elements are easily influenced by noise in the working environment that will lead to difficulty in the interpretation of the monitored signal. Wavelet analysis is therefore adopted for postprocessing of the raw monitored signal. As opposed to ordinary FFT analysis, wavelet analysis methods have both good time-frequency resolution and provide a constant bandwise frequency analysis.

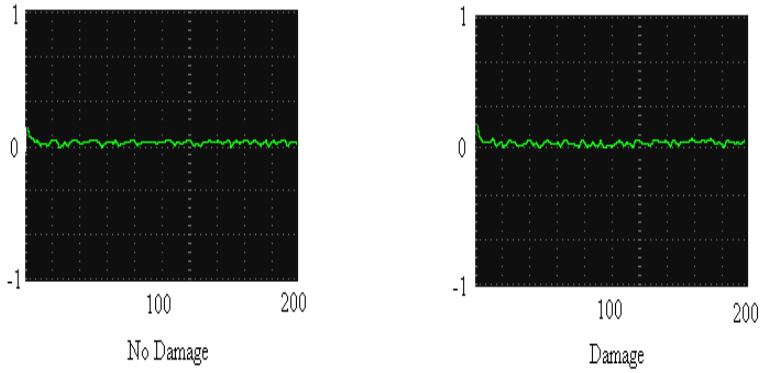

Figure 5.25: Signal after Postprocessing of Plate Specimen

5.4 Development of a New Signature

In order to effectively monitor damage in the structure, a reliable signature should be developed that is related only to damage. Many experiments show that the relationship between the highest peak amplitude and the propagating distance of the actively monitored signal in the structure can be described using an exponential relationship of the form:

$$A = A_0 e^{-\alpha x}$$

Where A= the peak amplitude of the actively monitored signal, x=the distance of signal propagation, α=attenuation coefficient,A_0=the initial peak amplitude value at the point of actuation. To reduce the propagation distance effect on peak value, a new signature can be defined as:

$$N_s = A_0 = \frac{A}{e^{-\alpha x}}$$

DOI : https://doi.org/10.56452/112

In fact, the newly-defined signature is the initial peak amplitude of the actively monitored signal, so it eliminates the propagation distance effect and emphasizes the effect of damage on the actively monitored signal.

5.5 Lamb Waves through Composite Plate:

Figure 5.26 represents the signal received at locations 2, 3, 4, 5, and 6 when the PWAS at 1 was excited in the frequency band 50-350 kHz. These signals traveled over the bond area, consisting of the Teflon layers plus the adhesive in between. However it is remarkable that signals of good quality and strength are observed in spite the small size of our PWAS devices. Also noticed in Figure 5.26 is how frequency affects the amplitude of the signal transmission. This aspect is important for designing PWAS installation that is tuned to certain Lamb modes.

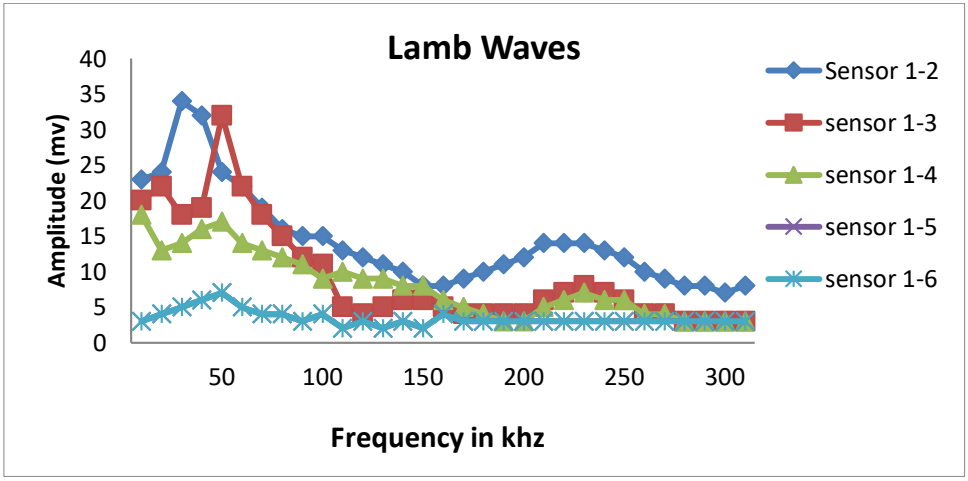

Figure 5.26: S0 and A0 Modes for Lamb Waves

Figure 5.26 shows that, at relatively low frequency, good signals are received. However, as indicated by the Lamb waver theory, these signals are of the flexural type (A0) and thus highly dispersive. Of considerable interest are the signals of axial type (S0), which have a lower dispersion rate, and hence are better suited to ultrasonic NDE. This fact is very encouraging because the S0 modes have very little dispersion at 200-260 kHz and hence could be used in the pulse-echo mode.

5.5.1. Effect of Change in Frequency on Signal Amplitude for Each Sensor Pair.

Frequency in (khz)	Signal Amplitude in (mv)				
	Sensor 1-2	sensor 1-3	sensor 1-4	sensor 1-5	sensor 1-6
10	24	21	19	3	3
20	24	22	13	4	4
30	34	18	14	5	5
40	32	19	16	6	6
50	24	22	17	7	7
60	22	22	14	5	5
70	19	18	13	4	4
80	16	15	12	4	4

DOI : https://doi.org/10.56452/112

90	15	12	11	3	3
100	15	11	9	4	4
110	13	5	10	2	2
120	12	4	9	3	3
130	11	5	9	2	2
140	10	6	8	3	3
150	8	6	8	2	2
160	8	5	6	4	4
170	9	4	5	3	3
180	10	4	4	3	3
190	11	4	3	3	3
200	12	4	3	3	3
210	14	6	5	3	3
220	14	7	6	3	3
230	14	8	7	3	3
240	13	7	6	3	3
250	12	6	6	3	3
260	10	4	4	3	3
270	9	4	4	3	3
280	8	3	3	3	3
290	8	3	3	3	3
300	7	3	3	3	3
310	8	3	3	3	3

Table 6: Effect of Change in Frequency on Signal Amplitude for Each Sensor Pair

5.6 Least Square Approach

To determine the new signature, a least-squares approach is employed structure peak-to-peak response for all of the actuator and sensor pairs on the structure that do not have damage between them, the values of$A0$ for the healthy structure and the coefficient a for a specimencan be calculated. Results of the least-squares curve-fittingmethod are shown in Figure.9.27Table shows the calculated $A0$ in a healthy state and $\boldsymbol{\alpha}$ coefficient for specimens.

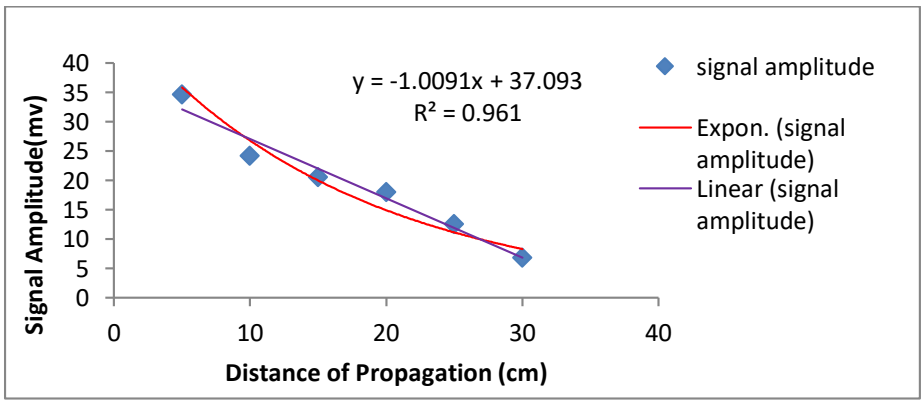

Figure 5.27: Effect of Distance of Propagation on Signal Amplitude.

DOI : https://doi.org/10.56452/112

Specimen	A0	A	Ns
Composite Plate Without Damage (7.5cm)	34.5	0.039	47.13
(19.5cm)	24		49.3
(26.7cm)	18		47.57

Table 7: New Damage Signature for Healthy Specimen without Delamination

5.7 RESULT TABLE

Signal Amplitude and Ns (Damage Index for Specimen)

(Comparing the damage signature of delaminated plates with damage signature of healthy specimen)

Specimen No.	Propagation Distance (cm)	Signal Peak Amplitude	Ns	Damage
1				
SPECIMEN WITH CENTERED SQUARE DELAMINATION	7.5 (sensor 1)	32.8	42.9	Yes
	19.5(sensor 2)	12.1	31.33	Yes
	26.7 (sensor 3)	8.04	20.49	Yes
2				
SPECIMEN WITH CENTERED TRIANGULAR DELAMINATION	7.5(sensor 1)	32.1	42.12	Yes
	19.5(sensor 2)	12.6	33.33	Yes
	26.7 (sensor 3)	8.6	20.9	Yes
3				
SPECIMEN WITH OUTLINE SQUARE DELAMINATION	7.5 (sensor 1)	32.5	42.6	Yes
	19.5(sensor 2)	22.18	44.75	Yes
	26.7 (sensor 3)	16.2	42.36	Yes

6. Conclusion and Future Scope.

The composite plate made of epoxy-fiberglass composite and one Teflon layer in the middle. The face sheets have higher stiffness, which is easier for the high frequency signal to propagate in while the composite plate has a higher ability to absorb the signal. So when delamination happens, the signal tends to travel more in the face sheet material, which reduces the high frequency components of signal that are absorbed. A new damage signature has been introduced to determine both the existence and the extent of damage; this signature is not sensitive to the distance between the active monitoring elements. Experiments have shown this signature to be

effective and readily-obtained. Based on this study, an online real-time active monitoring system for damage detection has been successfully established.

Some further researches need to be done to make this approach more practical, such as

1) Influence of the environment parameters.
2) Effect of different types of damages on lamb waves like hairline crack, corrosion, and surface mounted putty has to be study in further researches.
3) Perform additional experimental test with an increased number of specimens and with various types and sizes of damages for detecting actual size and shape of damage.

References

[1] Achenbach, J. D. (1973) "Wave Propagation in Elastic Solids", North Holland Pub. Co., Amsterdam.

[2] Alleyne, D. N.; Cawley, P.(1992) "The interaction of Lamb Waves with Defects", IEEE, Vol. 39, pp.381-397,

[3] Bruno ROCHA, Carlos SILVA, Afzal SULEMAN (2009) "Development of a PZT Phased Array and FBG Network for Structural Health Monitoring Based in Guided Lamb Waves" 2nd International Symposium on NDT in Aerospace.

[4] Crawley, E. A., and DeLuis, J., (1987), ''Use of Piezoelectric Actuators as Elements of Intelligent Structures,'' AIAA J, pp. 1375–1385.

[5] Keilers, C. H., and Chang, F-K., (1995), ''Identifying Delaminations in Composite Beams Using Built-in Piezoelectrics" Part I-Experiments and Analysis; Part II-An Identification Method,'' J. Intell. Mater. Syst. Struct., 6, pp. 649–672.

[6] Lester, H.C., Lefevre, S. (1993), "Piezoelectric actuator models for active sound and vibration control of cylinders", Journal of Intelligent Material Systems and Structures, v 4, pp 295-306

[7] Shenfang Yuan, Wang Lei, Lihua Shi (2003), "Active Monitoring for On-Line Damage Detection in Composite Structure"s. Journal of Vibration and Acoustics, Vol. 1250, pp 178-186

[8] Tzou, H.S., Tseng, C.I. (1991), "Distributed modal identification and vibration control of continua. Piezoelectric finite element formulation and analysis."Journal of Dynamic Systems, Measurement and Control. Transactions of the ASME, V 113,pp 500-505.

[9] Victor Giurgiutiu,(2000), "Active Sensors for Health Monitoring of Aging Aerospace Structures" International symposium on smart structures and materials and international symposium on nondestructive evaluation and health monitoring of aging in a structure. pp3985-4103.

[10] Yi Lu, Xin Wang, Jiong Tang (2007), "Robust Decision Making in Damage Detection Using Piezoelectric Transducers and Lamb Wave Propagation" Sensors and smart structures technologies for civil, mechanical and aerospace. Vol.6529.